

Diversity decoupled from ecosystem function and resilience during mass extinction recovery

Authors: Sarah A. Alvarez^{1,2,†*}, Samantha J. Gibbs³, Paul R. Bown², Hojung Kim², Rosie M. Sheward⁴, Andy Ridgwell⁵.

Affiliations:

¹School of Geographical Sciences, University of Bristol, University Road, Bristol, BS8 1SS, UK.

²Department of Earth Sciences, University College London, Gower Street, London, WC1E 6BT, UK.

³Ocean and Earth Science, National Oceanography Centre, Southampton, University of Southampton, Southampton, SO14 3ZH, UK.

⁴Institute for Geoscience, Goethe-Universität Frankfurt, Altenhöferallee 1, 60438 Frankfurt am Main, Germany.

⁵Department of Earth Sciences, University of California at Riverside, Riverside, California 92521, USA.

*Correspondence to: sarah.alvarez@unigib.edu.gi

†Current address: University of Gibraltar, Europa Point Campus, Gibraltar GX11 1AA.

The Chixulub bolide impact 66 million years ago drove near-instantaneous oceanic ecosystem collapse. Devastating diversity loss at the base of ocean food-webs likely triggered cascading extinctions across all trophic levels¹⁻³ and caused severe disruption of ocean biogeochemical function, especially the cycling of carbon between the surface and deep sea^{4,5}. The absence of sufficiently detailed biotic data spanning the post-extinction interval has limited our understanding of how ecosystem resilience and biochemical function was restored, with estimates of ‘recovery’ varying from <100 years to 10 million years⁶⁻⁸. Using a 13-million-year long nannoplankton time-series we show that post-extinction communities exhibited 1.8 million years of exceptional volatility before a more stable equilibrium community emerged displaying hallmarks of resilience. The transition to this new equilibrium-state community with a broader cell-size spectrum coincides with indicators of carbon cycle restoration and a fully functioning biological pump⁹. This finding implies a fundamental link between ecosystem recovery and biogeochemical cycling over timescales that are longer than those suggested by proxies of export production^{7,8} but far shorter than the return of taxic richness⁶. That species richness remained low as both community stability and biological pump efficiency re-emerged, suggests that ecological function rather than number of species is more critical to community resilience and biochemical function.

The end Cretaceous bolide impact stripped the ocean of diversity and biogeochemical function¹ more abruptly than any other mass extinction event, including the current anthropogenically-induced crisis. Following >90% species extinction in calcifying plankton³, the immediate aftermath of the impact saw oceans repopulated by aberrant communities dominated by ephemeral species, atypical in ecology, physiology and cell size⁹⁻¹¹. Over time a diverse, biochemically-functioning and resilient ecosystem was re-established. This wholesale re-assembly of the ocean ecosystem provides clues to the essential attributes that

44 underpin stable ecosystems and maintain robust ecological states and function^{12,13}. However,
45 assessments of when this ecosystem ‘recovery’ was achieved vary widely in definition and
46 duration. Export production proxies imply virtually instantaneous restoration of at least some
47 biogeochemical functionality (<100 years)^{7,8}, while the return of species richness to pre-
48 extinction levels suggests recovery 8-10 million years (Myr) later⁶. Here, we track the post-
49 extinction path to ecosystem restoration by building an exceptional, high-resolution 13-
50 million-year community record of calcareous nannoplankton, the dominant fossil-forming
51 primary producers. Much of the marine food-web leaves little or no fossil remains, but the
52 biomineralised exoskeletons of calcareous nannoplankton provide a remarkable proxy for
53 basal ecosystem health during past environmental change events (see ref. 3 and refs therein).
54 Our new nannoplankton record bridges the temporal range of current recovery estimates and
55 allows us to target measures of community *stability* (the level of deviation around the average
56 state, see Methods) and *resilience* (the ability to resist and recover from perturbation¹⁴) as
57 they re-emerged. The record from Ocean Drilling Program (ODP) Site 1209 in the Pacific
58 Ocean (Extended Data Fig. 1, Methods) has highly-resolved orbital age control (see Methods)
59 and complementary proxy data for environmental change and biogeochemical function. Our
60 plankton data comprise a sample every ~13 thousand years, spanning 13 Myr, with around
61 700,000 fossil counts providing an unprecedented time-series of key community parameters,
62 including abundance, diversity, taxic richness, variance, dissimilarity and body size (see
63 Methods).

64 Our data and analyses reveal striking temporal trends in nannoplankton community structure
65 and resilience (Fig. 1). Most visually obvious is the differentiation of a highly volatile post-
66 extinction interval of ~1.8 Myr, from a subsequent more ‘stable’ background state (Fig. 1e),
67 conspicuous in the Summed Coefficient of Variation metric (Σ_{CV}). We primarily focus on this
68 metric which quantifies the level of variance or ‘stability’ in relative abundances (see
69 Methods) but as community stability is a multi-faceted concept, we also refer to other indices
70 including community dissimilarity (Bray-Curtis Dissimilarity) and diversity (Simpson’s
71 index of dominance/evenness). These measures of community structure all point to the state-
72 shift ~1.8 Myr post-impact (Fig. 1, Extended Data Fig. 2) and an early Danian interval
73 characterized by exceptional fluctuations that are statistically distinct from the rest of the
74 record (Extended Data Fig. 2), hereafter referred to as Regime 1 (66.0-64.2 Myr ago) and
75 Regime 2 (64.1-53.0 Myr ago). When we compare Σ_{CV} with carbon isotope ($\delta^{13}C$) excursion
76 magnitude, a proxy for environmental change (Fig. 2, see Methods), the two regimes show
77 strikingly different relationships with environmental forcing. The earliest Danian (Regime 1)
78 exhibits no relationship between Σ_{CV} and $\delta^{13}C$ magnitude, with prolonged high-amplitude
79 variance largely the statistical impact of a series of ocean-wide abundance acmes^{10,15,16} (Fig.
80 3a, b, Extended Data Figs 3, 4), occurring alongside very little apparent environmental
81 perturbation (Fig. 1a, 2). This interval saw very short-term (<<100 kyr) impact-related
82 environmental changes^{17,18} (cooling over <50 years, ref 17, and warming through <100 kyr,
83 ref 18), waning Deccan trap volcanism over 600 kyr (e.g., ref. 19), and only two notable
84 environmental change events – the lower-C29n and Dan-C2 hyperthermals - all occurring or
85 ceasing well before the interval of high variance comes to an end. Therefore, the disconnect
86 between community metrics and indicators of climate variability suggests that environmental
87 changes were not driving and maintaining the high levels of biotic variability through this
88 1.8-million-year interval. In contrast, above this level (Regime 2), $\delta^{13}C$ magnitude is a strong
89 predictor of community variance ($R^2 = 54\%$ on first differences, Fig. 2) with the majority of
90 data forming a ‘background’ grouping punctuated by variance peaks associated with
91 hyperthermal events²⁰ (highlighted in red in Figs 1a, c, Fig. 2). This indicates that by the late
92 Danian, nannoplankton communities were fluctuating around some steady state and

93 demonstrate indicators of resilience¹⁴, including proportionate responses to environmental
94 perturbation (i.e., the significant linear trend between carbon isotope excursion and variance)
95 and rapid recoveries following each event (return of variance to the background state within
96 <200 kyrs of the excursion, Fig. 1c and ref 21).

97 Tantalisingly, the shift to more stable communities approximately 64.2 Myr ago (the end of
98 Regime 1) also falls towards the top of the interval of biological pump recovery⁹ (Fig. 3f).
99 Ocean biogeochemical function was profoundly disrupted by the end-Cretaceous mass
100 extinction, most obviously through weakening of the biological pump^{2,5,9}. The scale and
101 duration of this productivity reduction is contentious, ranging from scenarios of a lifeless
102 *Strangelove Ocean* to a partially functioning *Living Ocean* state⁴, but the long, multimillion-
103 year delay in restoration of the biological pump is well established^{2,22}, and indicated by both
104 the gradual increase in vertical carbon isotope gradient to pre-extinction values⁹ and changing
105 community structures of benthic primary-consumer communities (benthic foraminifera)²³.
106 Carbon isotope gradients finally returned to pre-extinction values by ~1.77 Myrs after the
107 event⁹ providing an upper limit on full recovery of the biological pump. This broad
108 concurrence between biological pump restoration and the shift to a more stable plankton
109 community background state (Fig. 3) provides strong evidence for an intrinsic link between
110 biological recovery of the ecosystem and its calibre of biochemical functioning. We can
111 augment this understanding of ecosystem recovery and efficient biological pumping by
112 exploring the roles of the post-extinction taxonomic rebuild and rapid cell-size increases
113 using new, high-resolution species richness data (Fig. 3d; see Methods) and reconstructions
114 of nanoplankton community cell volume (Fig. 3e; see Methods).

115 Mean community cell volume and species richness exhibit pulsed patterns through the
116 Danian, both showing rapid increases in the first half million years after the mass extinction,
117 from initially extremely low species numbers and predominantly very small cells (Fig. 3d, e).
118 Rapid diversification within Regime 1 saw the appearance of >15 species alongside a peak in
119 cell volume around 300 kyr after the extinction level dominated by cells of heavily calcified
120 calcareous dinoflagellates. A second phase of cell-volume increase occurred as carbon export
121 gradually returned to pre-extinction values, and was driven by both diversity and ecology,
122 with relative abundance increases in existing large taxa (such as *Coccolithus*, Extended Data
123 Fig. 3) and the addition of larger new species across all of the emerging clades (Fig 3d).
124 Modern observations indicate that phytoplankton community size structure is a critical
125 control on export flux and, further, that nanoplankton mineral ballasting significantly
126 increases the transfer efficiency of carbon²⁴⁻²⁶. The shift to larger cells and ballast biominerals
127 seen in our early Danian cell size record (Fig. 3e) would therefore have contributed to
128 increased carbon export flux with stable, diverse communities delivering this flux more
129 consistently through space and time, and supporting greater size diversity in the
130 zooplankton²⁶. The role of larger zooplankton and the production of fast-sinking faecal
131 pellets in these evolving export pathways is more difficult to reconstruct due to poor fossil
132 records. However, an indication of higher trophic level disruption is seen in the early Danian
133 zooplanktonic foraminifera where low diversities, acme fluctuations and small body size are
134 observed across similar timescales to the recovery of the biological pump^{11,27}. Finally, a third
135 phase of cell volume increase coincides with a major expansion of ecological diversity
136 marked by the appearance of the first specialist oligotrophic nanoplankton since the mass
137 extinction (Discoasterales; ~3.5 Myr post-extinction; Figs 1b, 3a, d, e, Extended Data Fig. 4;
138 ref 28) and re-introduction of photosymbiotic strategies in planktonic foraminifera (~2.5 Myr
139 post-extinction; Fig. 3f; ref 9). Diversification then continued, with species richness only
140 reaching pre-extinction levels at 10 Myr after the mass extinction (~56 Myr ago; Fig. 1g).

141 The scale of ecosystem collapse at the K/Pg event and protracted recovery of resilience,
142 diversity and biogeochemical function, demonstrates the singular consequences of mass-
143 extinction-level change and subsequent durability of ecosystems following restoration.
144 Predictions of contemporary mass-extinction²⁹ detail accelerating declines in ecosystem
145 functioning as diversity falls^{30,31}. We show here that this relationship also holds in reverse as
146 biodiversity reboots after a mass extinction. Early but modest taxic and trait (especially size)
147 diversification within the recovering biota re-established ecosystem stability with links to
148 functioning (specifically the biological pump) long before species richness and ecological
149 diversity returned to pre-extinction levels. Rapid biotic turnover and community instability
150 during this reboot increased the probability of biotically-forced evolution alighting on
151 organisms capable of fulfilling essential functional roles, which in turn facilitated community
152 recovery and the re-emergence of ecosystem stability. Ecosystem stability is therefore not
153 determined by sheer numbers of species, but rather through the establishment and/or retention
154 of key functional taxa fulfilling vital ecological and/or biogeochemical roles.

155 **References:**

- 156 1. Schulte, P. *et al.* The Chicxulub asteroid impact and mass extinction at the Cretaceous-
157 Paleogene boundary. *Science*. **327**, 1214–1218 (2010).
- 158 2. Coxall, H. K., D’Hondt, S. & Zachos, J. C. Pelagic evolution and environmental
159 recovery after the Cretaceous-Paleogene mass extinction. *Geology* **34**, 297–300
160 (2006).
- 161 3. Bown, P. R., Lees, J. A. & Young, J. R. Calcareous nannoplankton evolution and
162 diversity through time. in *Coccolithophores: from molecular processes to global*
163 *impact* (eds. Thierstein, H. R. & Young, J. R.) 481–508 (Springer, 2004).
- 164 4. D’Hondt, S. Consequences of the Cretaceous/Paleogene mass extinction for marine
165 ecosystems. *Annu. Rev. Ecol. Evol. Syst.* **36**, 295–317 (2005).
- 166 5. Henehan, M. J., Hull, P. M., Penman, D. E., Rae, J. W. B. & Schmidt, D. N.
167 Biogeochemical significance of pelagic ecosystem function: an end-Cretaceous case
168 study. *Philos. Trans. R. Soc. B* **371**, 20150510 (2016).
- 169 6. Kirchner, J. W. & Weil, A. Delayed biological recovery from extinctions throughout
170 the fossil record. *Nature* **404**, 177–180 (2000).
- 171 7. Sepúlveda, J., Wendler, J. E., Summons, Roger, E. & Hinrichs, K.-U. Rapid
172 Resurgence of Marine Productivity After the Cretaceous-Paleogene Mass Extinction.
173 *Science*. **326**, 129–132 (2009).
- 174 8. Alegret, L., Thomas, E. & Lohmann, K. C. End-Cretaceous marine mass extinction not
175 caused by productivity collapse. *Proc. Natl. Acad. Sci.* **109**, 728–732 (2012).
- 176 9. Birch, H. S., Coxall, H. K., Pearson, P. N., Kroon, D. & Schmidt, D. N. Partial
177 collapse of the marine carbon pump after the Cretaceous-Paleogene boundary.
178 *Geology* **44**, 287–290 (2016).
- 179 10. Bown, P. Selective calcareous nannoplankton survivorship at the Cretaceous-Tertiary
180 boundary. *Geology* **33**, 653–656 (2005).
- 181 11. Gallala, N., Zaghib-Turki, D., Arenillas, I., Arz, J. A. & Molina, E. Catastrophic mass
182 extinction and assemblage evolution in planktic foraminifera across the
183 Cretaceous/Paleogene (K/Pg) boundary at Bidart (SW France). *Mar. Micropaleontol.*

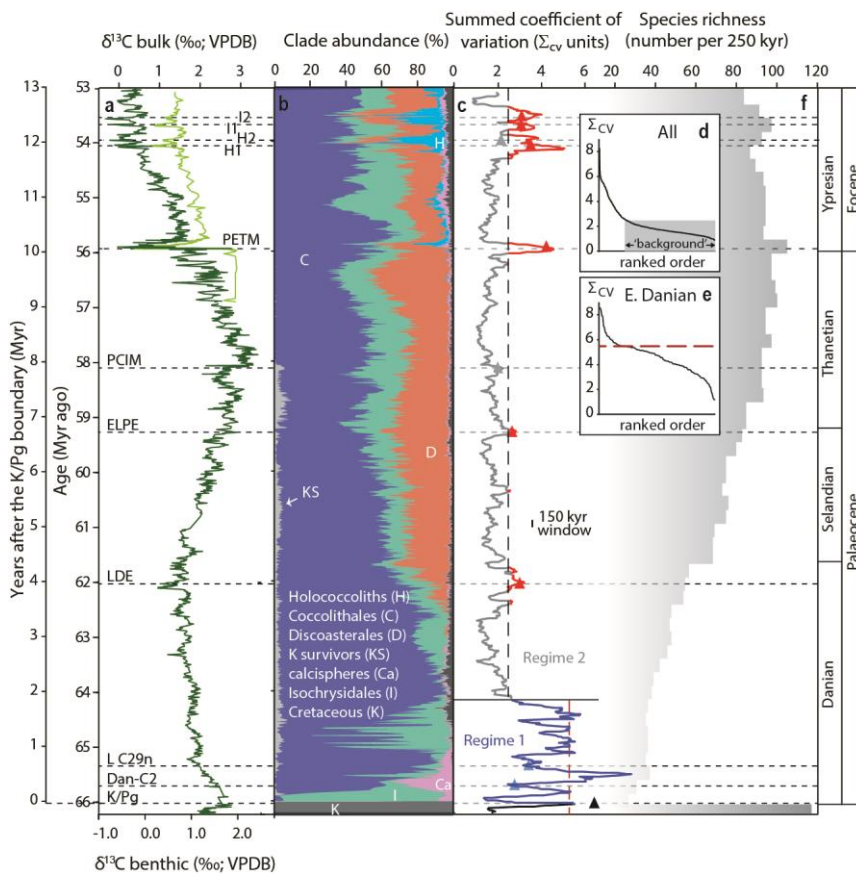
- 184 **72**, 196–209 (2009).
- 185 12. P. Hull, Life in the aftermath of mass extinctions. *Curr. Biol.*, **25**, R941–R952 (2015).
- 186 13. Barnosky, A. D., *et al.* Merging paleobiology with conservation biology to guide the
187 future of terrestrial ecosystems. *Science* **355** (2017)
- 188 14. Hodgson, D., McDonald, J. L. & Hosken, D. J. What do you mean, ‘resilient’? *Trends*
189 *Ecol. Evol.* **30**, 503–506 (2015).
- 190 15. Varol, O. Palaeocene calcareous nannofossil biostratigraphy. in *Nannofossils and their*
191 *Applications* (eds. Crux, J. A. & van Heck, S. E.) 267–310 (Ellis Horwood, British
192 Micropaleontological Society Series, 1989).
- 193 16. Pospichal, J. J. Calcareous nannoplankton mass extinction at the Cretaceous/Tertiary
194 boundary: An update. in *The Cretaceous-Tertiary Event and Other Catastrophes in*
195 *Earth History. Geological Society of America Special Paper 307* (eds. Ryder, G.,
196 Fastovsky, D. E. & Gartner, S.) 335–360 (1996).
- 197 17. Vellekoop, J. *et al.* Rapid short-term cooling following the Chicxulub impact at the
198 Cretaceous-Paleogene boundary. *Proc. Natl. Acad. Sci.* **111**, 7537–7541 (2014).
- 199 18. MacLeod, K. G., Quinton, P. C., Sepúlveda, J. & Negra, M. H. Postimpact earliest
200 Paleogene warming shown by fish debris oxygen isotopes (El Kef, Tunisia). *Science*.
201 **360**, 1467–1469 (2018).
- 202 19. Sprain, C. J. *et al.* The eruptive tempo of Deccan volcanism in relation to the
203 Cretaceous-Paleogene boundary. *Science* **363**, 866-870 (2019).
- 204 20. Zachos, J. C., McCarren, H., Murphy, B., Röhl, U. & Westerhold, T. Tempo and scale
205 of late Paleocene and early Eocene carbon isotope cycles: Implications for the origin
206 of hyperthermals. *Earth Planet. Sci. Lett.* **299**, 242–249 (2010).
- 207 21. Gibbs, S. J. *et al.* Scaled biotic disruption during early Eocene global warming events.
208 *Biogeosciences* **9**, 4679–4688 (2012).
- 209 22. Esmeray-Senlet, S. *et al.* Evidence for reduced export productivity following the
210 Cretaceous/Paleogene mass extinction. *Paleoceanography* 10.1002/2014PA002724
211 (2015).
- 212 23. Alegret, L. & Thomas, E. Deep-Sea environments across the Cretaceous/Paleogene
213 boundary in the eastern South Atlantic Ocean (ODP Leg 208, Walvis Ridge). *Mar.*
214 *Micropaleontol.* **64**, 1–17 (2007).
- 215 24. Buesseler, K.O. & Boyd, P.W. Shedding light on processes that control particle export
216 and flux attenuation in the twilight zone of the open ocean. *Limnol. Oceanogr.* **54**,
217 1210–1232 (2009).
- 218 25. Fischer, G. & Karakaş G., Sinking rates and ballast composition of particles in the
219 Atlantic Ocean: implications for the organic carbon fluxes to the deep ocean.
220 *Biogeosciences* **6**, 85–102 (2009).
- 221 26. Hansen, B., Bjørnsen, P., K. & Hansen, P.J. *et al.* The size ratio between planktonic
222 predators and their prey. *Limnol. Oceanogr.* **39**, 395-403 (1994).
- 223 27. Gerstel, J., Thunell, R. & Ehrlich, R. Danian faunal succession : Planktonic
224 foraminiferal response to a changing marine environment. *Geology* **15**, 665–668

- 225 (1987).
- 226 28. Fuqua, L. M., Bralower, T. J., Arthur, M. A. & Patzkowsky, M. E. Evolution of
227 calcareous nannoplankton and the recovery of marine food webs after the Cretaceous-
228 Paleocene mass extinction. *Palaios* **23**, 185–194 (2008).
- 229 29. Barnosky, A. D. *et al.* Has the Earth's sixth mass extinction already arrived? *Nature*
230 **471**, 51–57 (2011).
- 231 30. Cardinale, B. J. *et al.* Biodiversity loss and its impact on humanity. *Nature* **486**, 59–67
232 (2012).
- 233 31. Reich, P. B. *et al.* Impacts of biodiversity loss escalate. *Science*. **336**, 589–592 (2012).
- 234 32. Westerhold, T., Röhl, U., Donner, B. & Zachos, J. C. Global extent of early Eocene
235 hyperthermal events – a new Pacific benthic foraminiferal isotope record from Shatsky
236 Rise (ODP Site 1209). *Paleoceanogr. Paleoclimatology* **33**, 626–642 (2018).
- 237
- 238

239 **Figures:**

240 **Figure 1. Nannoplankton abundance, variability and diversity records from the latest**
 241 **Cretaceous to early Eocene.** **a**, Carbon stable isotopes, dark green – benthic³², lighter green
 242 - bulk (see references in 21). **b**, Summary of main nannoplankton clade abundances
 243 determined for 981 samples. **c**, Summed coefficients of variation (Σ_{CV}) using 150 kyr moving
 244 window (see Methods), separated into the early Danian (Regime 1, blue) and the rest of the
 245 record (Regime 2, grey and red). The Cretaceous to K/Pg data points are in black. Triangles
 246 (colour-coded by regime, black for the K/Pg window) show values for the named climate
 247 events, which for the Eocene hyperthermals were calculated across the event duration (<150
 248 kyr). Event nomenclature follows references given in the Methods. The vertical black dashed
 249 line indicates estimated background level (<2.5 Σ_{CV}) based on the ranked order
 250 point on **(d)** with above-‘background’ data highlighted in red in **c**. **e**, Ranked-order plot of
 251 Regime 1 datapoints where the dark red dashed line indicates an inflection point at the higher
 252 end of the Σ_{CV} values (marked on **c**). **f**, Calcareous nannoplankton species richness at 250 kyr
 253 resolution (see Methods).

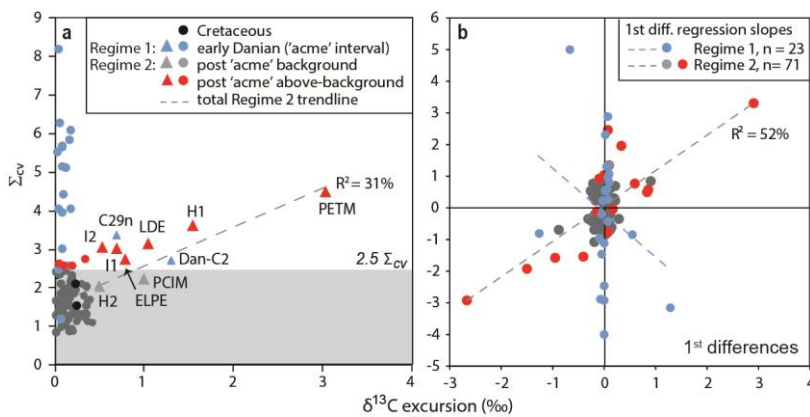
254



255
 256

257 **Figure 2. Σ_{CV} and magnitude of climate perturbation ($\delta^{13}C$ excursion).** **a**, raw data. **b**,
 258 first differences. The Σ_{CV} values are plotted for each named climate event (using the
 259 highlighted values in Fig. 1c, here shown as triangles in **a**) and every intervening ~ 150 kyr.
 260 Data-points are separated into Cretaceous (black, $n = 2$, not included in **b**), early Danian
 261 (blue, 66 to 64.2 Myr ago, Regime 1, $n = 23$) and the rest of the record (grey and above
 262 background in red, Regime 2, $n = 71$, from Fig. 1c, d). Regime 1 Σ_{CV} shows no relationship
 263 with climatic perturbation (blue trend-line in **b**), unlike Regime 2 (generalised least squares
 264 trend-line for all grey plus red data-points, $n = 71$, grey dashed line in **a** and **b**), which is
 265 significant in both the raw data (**a**) and on first differences (**b**) ($R^2 = 31\%$ and 52% ,
 266 respectively (see Methods). The inferred background level of 2.5, based on rank ordering
 267 (Fig. 1d), is indicated by the grey box.

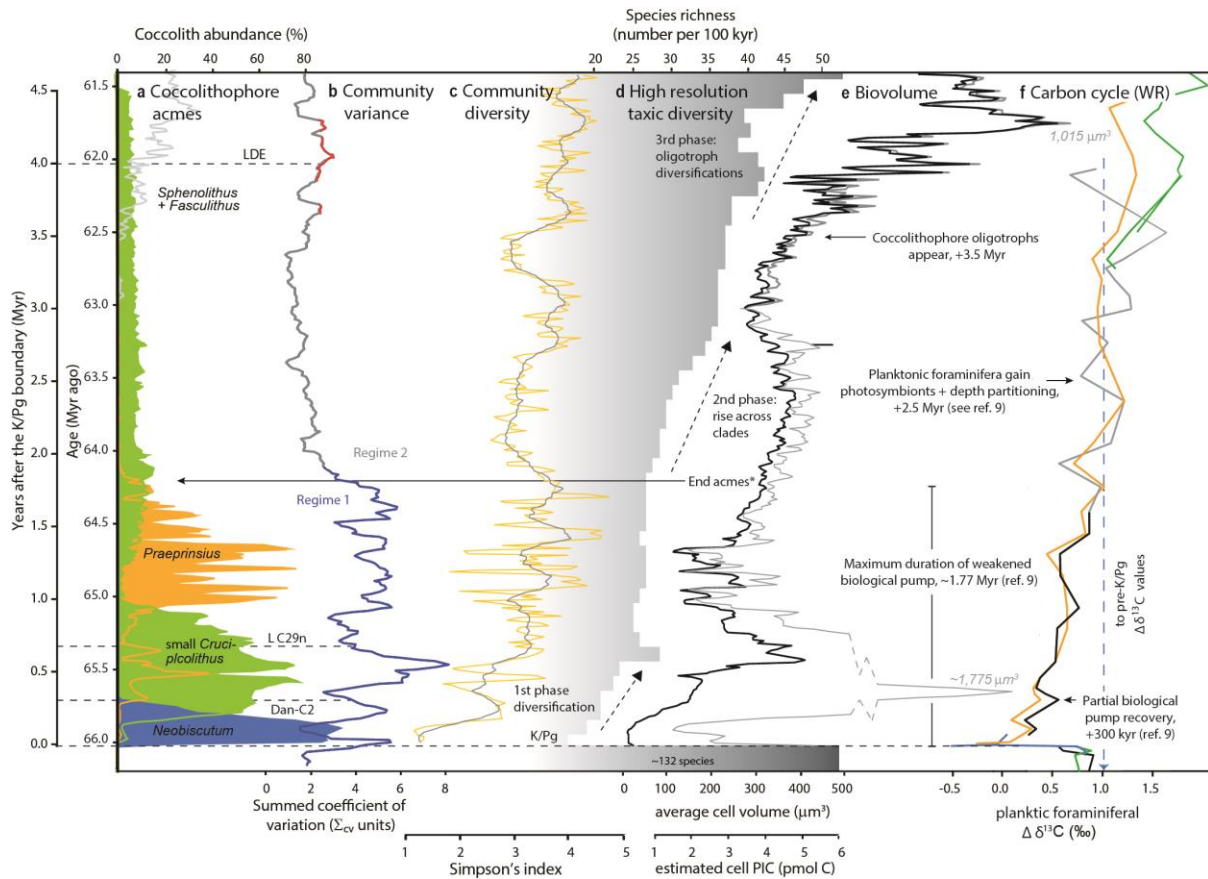
268



269
 270

271 **Figure 3. Danian nannoplankton community variance, acme abundances, diversity, cell**
 272 **volume and key milestones. a,** Abundance records of the early Danian coccolithophore
 273 acmes and Discoasterales (*Sphenolithus* and *Fasciculithus*), **b,** Σ_{CV} (Regime 1 in blue,
 274 Regime 2 in grey and red) and Danian climate events. **c,** Community diversity (Simpson's
 275 index), 150 kyr moving average in grey. **d,** Global species richness resolved at 100 kyr scale
 276 (see Methods). **e,** Estimated average (mean) cell volume and estimated particulate inorganic
 277 carbon content (PIC) of the calcareous nannoplankton (grey), excluding calcispheres (black)
 278 (see Methods). Cell size maxima at 300 kyr and 4.25 Myr after the K/Pg given in grey italics.
 279 Key milestones/observations from herein and from published records are indicated (see
 280 Methods). *The level for the end acmes is taken as the top of the *Praeprinsius* acme. **f,**
 281 Carbon isotope gradient ($\Delta\delta^{13}C$) between Walvis Ridge (WR, ODP Site 1262) planktonic and
 282 benthic foraminifera species (ref 9, using adjustment option 2), grouped according to ecology
 283 (blue – surface survivors, green – surface symbiotic, orange – thermocline, black – mixed
 284 layer, grey – transitional).

285



286
287

288 **METHODS**

289 **Experimental Design.** Our objective was to characterize the emergence of resilience in
290 plankton communities in the aftermath of the Cretaceous-Palaeogene (K/Pg) mass extinction
291 and assess implications for higher trophic levels and biogeochemical cycling of the oceans.
292 This work is the first palaeoecological study to present sustained very-high resolution
293 sampling (13 kyr) over such a long duration (13 million years), maintaining sampling
294 intensity across both event and background stratigraphic intervals. To achieve this, we
295 required a continuous long time-series record from a single location that was representative
296 of global patterns, all features satisfied by the open ocean, gyre location of Ocean Drilling
297 Program (ODP) Site 1209. The palaeogeography and overall oceanic setting varied little at
298 this site across the 13 Myr record and calcareous nannoplankton provide the most consistent,
299 high abundance fossil record of nannoplankton. This site has an orbitally-resolved age model,
300 providing millennial sampling precision alongside high-resolution geochemical proxy records
301 of palaeoenvironmental change³¹. Furthermore, the site is far from the Yucatan bolide impact
302 and samples the dominant ocean basin of the early Cenozoic, providing the potential to track
303 marine ecosystem recovery on a quasi-globally representative basis (see *cGENIE* section
304 below).

305 **Sampling strategy.** The nannoplankton assemblage data come from a ~54 metre section of
306 the composite splice³³ at ODP Site 1209 Shatsky Rise, in the palaeo-subequatorial Pacific
307 Ocean (Extended Data Fig. 1). 981 samples were taken at ~13 kyr intervals, extending from
308 the K/Pg boundary (66 Myr ago) through to the Palaeocene-Eocene Thermal Maximum
309 (PETM: 56 Myr ago) and overlap the Eocene record of ref 21, giving a 13-Myr long record in
310 total. Ages assigned to each sample use age models constructed for ODP Site 1209 by ref 34
311 and ref 35 (option 2), updated by ref 32. The age model uses tie-points in the $\delta^{13}\text{C}$ data
312 correlated with the orbitally-tuned stratigraphy of ODP Site 1262, as summarized by ref 20
313 and ref 32.

314 **Assemblage data.** Smear slides were prepared for nannofossil observation using standard
315 techniques³⁶. Assemblage data (Extended Data Fig. 3) are based on statistically significant
316 counts of 500 to 1000 nannofossil liths per sample across a minimum of 10 fields of view,
317 following identical count and taxonomic protocols of the Eocene record from ref 21 (~218.5
318 to 208.0 rmcd, ~56 to 53 Ma). The assemblage data were counted to generic level, with some
319 additional division into useful morphogroups (e.g., determined by genus and size, see below).
320 Taxonomy generally follows refs 37–39. Visual assessment of preservation, as well as
321 quantitative counts of lith fragmentation and presence of delicate lith structures, indicates that
322 the nannofossils are generally well preserved but show some signs of etching and minor
323 overgrowth, as is typical for carbonate-rich deep-sea sediments. Etching of delicate central
324 area structures, particularly of Prinsiacae specimens is common, but does not inhibit
325 identification to genus level. While there is always some degree of variation in preservation
326 quality through a long time-series such as this, our observations show that dissolution has not
327 disproportionately distorted the assemblage character at any particular level or interval. This
328 includes the hyperthermals where carbonate dissolution often increases (see ref 21) and,
329 conversely, the immediate post-K/Pg interval where indicators suggest enhanced
330 preservation⁴⁰. Of note, the later absence of the exclusively-small taxa, *Neobiscutum*, small
331 *Praeprinsius* and *Futyania*, is an evolutionary signal confirmed in sections worldwide¹⁵,
332 rather than a preservational artefact. There is evidence of reworking of Cretaceous taxa

333 immediately above the K/Pg boundary at Site 1209 (Extended Data Fig. 3), but these
334 specimens have not been included in the relative abundance calculations.

335 **Summed coefficient of variation (Σ_{CV}).** We have used a range of approaches (see below) to
336 characterise community structure but focus on the Σ_{CV} time-series as it best encapsulates the
337 key trends in community variance and relationships with environmental perturbation. The
338 Σ_{CV} method is an analytical technique that is independent of taxic composition, and enables
339 efficient collection and integration of large amounts of abundance data giving equal
340 weighting to each of the taxa included²¹. When applied to microfossil data, it highlights the
341 nuances of biotic response across a very broad spectrum of perturbations. We follow the
342 same procedure as ref 21 but without using the SiZer smoothing step because we are not
343 comparing datasets from different sources. First, the assemblage data, collected from samples
344 taken every ~5.5 cm (equivalent to every 13 kyr) were placed on the age scale and linearly
345 resampled using *AnalySeries version 2.0*⁴¹ to provide consistent 13 kyr spacing between
346 datapoints. Second, we determined which taxa would be included for subsequent Σ_{CV}
347 analysis. Because the 13 Myr record includes significant evolution in community taxon-
348 makeup, we divided the section into million-year bins and determined the most abundant and
349 consistently present (>65% of samples) taxa in each. This resulted in the selection of 8 taxa
350 across each bin - a relatively low number because of the low diversity in the early Danian but
351 representing >95% of the total population in each sample. We then followed the Σ_{CV} method
352 of calculating coefficients of variation summed across these taxa using a moving window
353 duration of 150 kyrs. As the Σ_{CV} metric quantifies the levels of variance across multiple taxa,
354 our use of the term stability here refers to consistent and low levels of change in the
355 abundance distribution across the main taxa. The term stability is used in ecology in a myriad
356 of ways but in this case, we use a simple and intuitive definition of stability as meaning a
357 system with low variability (i.e., little deviation from its average state; following ref 42) - a
358 definition we think is most directly applicable to geological time-series data.

359 **Σ_{CV} sensitivity tests.** We have applied a range of sensitivity tests to the Σ_{CV} metric record,
360 examining for the effects of sample window duration, taxon dominance, ancestry, fossil
361 preservation, sedimentation rate and hiatuses (see also ref 21). Extended Data Figure 5
362 explores the impact of varying window duration and reveals how variance is packaged
363 through time, as well as any differences resulting from analysing the data in time *versus* age
364 domains. Σ_{CV} *increases* with increasing window-duration in the lower Danian, indicating that
365 the window is capturing additional variance that is spread throughout the interval. By
366 contrast, Σ_{CV} *decreases* with increasing window-duration across the PETM and ETM2,
367 indicating focused variance, with little additional variance in the broader time window
368 diluting the signal. We have explored the impact of shared ancestry because our analyses give
369 equal weight to each taxonomic unit potentially introducing artificially high variance. We
370 have tested for this by re-analysing the data using two additional models of shared ancestry
371 developed from our genus-level stratophenetic tree (Extended Data Fig. 6). Sensitivity of the
372 Σ_{CV} metric decreases as more genera are grouped, damping levels of variance (Extended Data
373 Fig. 7), particularly when merging abundant genera from the same family (the highly
374 conservative ancestry Option 1). However, the main patterns of variance still remain as
375 robust features (as they do in the dissimilarity index described below), particularly when
376 more branches of the tree are conserved (the moderately conservative ancestry Option 2).

377 **Dissimilarity and diversity metrics.** We have calculated additional metrics of assemblage
378 structure, namely Bray-Curtis Dissimilarity (BC; a metric that highlights structural
379 differences in abundance and composition); the Simpson's index (SI; an evenness/dominance
380 metric that incorporates abundance distribution and taxic richness), and the standard
381 deviation (variance) of the SI (Extended Data Fig. 2). BC was performed on the maximum
382 and minimum abundance values across the 11 samples within each moving 150 kyr window,
383 returning the maximum dissimilarity value. The values have been plotted for each moving
384 150 kyr window through the time-series. BC is sensitive to taxonomic turnover (shown by
385 increasing values with increasing window size, Extended Data Fig. 5b) but the impact is
386 minimised using the 150 kyr window, as species turnover is low. The standard deviation
387 (variance) of SI was calculated from the 11 samples in each 150 kyr moving window. The
388 Σ_{CV} and BC time-series patterns are very similar (R^2 of 63%) but the BC record differs in the
389 amplitude of variation through background intervals because it is influenced, to varying
390 degrees through the time-series, by rare taxa. SI is also highly sensitive to rarer taxon
391 abundances and the rare, variable occurrences of taxa close to their appearance and/or
392 disappearance.

393 **Species richness estimates.** The new species richness diversity data is an update of the
394 global compilation of ref 3. We have added new taxa described since 2004, increased the
395 temporal resolution to 250 kyr stratigraphic bins for the entire dataset (Fig. 1 and Extended
396 Data Fig. 4) and 100-kyr bins for the Danian (Fig. 3), and present the data on the GTS2012
397 timescale⁴³. The species richness is the total number of taxa that occur for some part of, or
398 throughout, each stratigraphic bin. Species richness estimates are dependent on the bin
399 duration, hence the difference between the values in Figures 1f and 3d.

400 **Cell size and volume.** Estimates of average cell volume (Fig. 3 and Extended Data Fig. 4)
401 are based on mean cell size per taxon weighted according to their abundance in the
402 community at any given time.

403 Average cell volume = $\frac{((\%T1_{ra} \times \Theta T1_{av}) + (\%T2_{ra} \times \Theta T2_{av}) + (\%T3_{ra} \times \Theta T3_{av}) \dots T_n)/2^3}{3 \times 4\pi} / \Sigma \%T_{ra}$

404 Where % $T1_{ra}$ is the % relative *cellular* abundance of the taxon in the total assemblage and
405 $\Theta T1_{av}$ is the average cell diameter of the taxon.

406 Cell diameter uses the internal diameter of coccospheres and cellular abundances were
407 estimated by dividing the relative abundance of liths present by the average number of liths
408 per cell. Coccosphere size and lith number for each taxon use (i) direct coccosphere
409 measurements from coeval samples at ODP Site 1209 (Shatsky Rise), and also from
410 Integrated Ocean Drilling Program (IODP) Sites 1403 and 1407 (North Atlantic), and from
411 published scanning electron microscope (SEM) images of coccospheres^{44,45}; (ii) coccolith
412 measurements from these same samples converted to estimated cell size (and associated lith
413 number) based on taxon-specific relationships between lith size, lith number and cell size
414 determined from Palaeogene taxa within the same genus or family⁴⁶; or (iii) estimates using
415 modern analogues⁴⁶ (details in Extended Data Table 1). For the calcareous dinocysts, we took
416 a conservative estimate of cell diameter of 20 microns, based on light microscope and SEM
417 images of complete dinocyst coverings from the lowermost Danian of ODP Site 1210
418 (Shatsky Rise) and divided raw calcareous dinocyst fragment counts by 12, as an estimate of
419 how many fragments constitute a whole cell. Estimated particulate inorganic carbon per cell
420 uses the least-squares linear regression between cell volume and cell PIC in Figure 4c of ref.
421 46.

422 **cGENIE Earth system modelling and palaeo-hydrographic location of Site 1209.** We
423 illustrate the palaeo-hydrographic location of Site 1209 using the ‘cGENIE’ Earth system
424 model. In this simulation, cGENIE is configured with late Maastrichtian boundary conditions
425 of continental configuration, bathymetry, and wind stress as described in ref 47. Additionally,
426 the solar constant is reduced appropriate for 66 Myr ago and atmospheric CO₂ is set to 1112
427 ppm (×4 pre-industrial). We take the 10 kyr spin-up described in ref 47 and run this on for 10
428 more years, showing the results of the last year of the 10-year follow-on experiment in
429 Extended Data Figure 1 as an annual average. ODP Site 1209 was slightly to the north (ca.
430 8°) of the palaeo-Equator 66 Myr ago (Extended Data Fig. 1a), lying towards the edge of an
431 ocean current field that is circumequatorial (Extended Data Fig. 1b) and links the major
432 ocean basins. In the simulated late Maastrichtian climate, temperatures do not fall more than
433 about 6°C cooler than those at the location of Site 1209 (35°C), nor exceed this, anywhere
434 along the flow path by more than a few degrees C. Further, from simple visual inspection of
435 the cGENIE simulations (Extended Data Fig. 1), the deflection of the circumequatorial
436 current south of China and SE Asia to latitudes of ca. 10°S and interaction with the South
437 Pacific subtropical gyre, suggest the potential for significant surface-water mixing to occur
438 between the hemispheres. We conclude from this that Site 1209 is likely to be sampling the
439 same tropical and partly sub-tropical plankton communities that occur in all major ocean
440 basins and both hemispheres. The area of connected waters in the 28-38°C range is over 50%
441 of the global ocean surface. The obvious exceptions to this global connectivity are the Arctic
442 (being characterized by much cooler temperatures) and the South Atlantic (which exchanges
443 with the Pacific primarily only to the South of Africa, with the cooler water regime in this
444 ocean gateway representing a potential barrier to the mixing of tropical plankton communities
445 globally).

446 **Palaeogene climate events.** A number of significant climate events occur through the 13
447 Myr study interval, including named transient events marked by isotopic excursions and
448 identified on Figures 1 and 3, with further details provided in Extended Data Table 2. These
449 are mainly global warming hyperthermal events identified by carbon and oxygen isotope
450 excursions and associated deep-sea carbonate dissolution. Events I2, I1, H2, H1 and the
451 PETM were recognised at ODP Site 1209 by examination of benthic and bulk carbon isotope
452 values and magnetic susceptibility data, following refs 21 and 32. The PETM was also
453 identified in benthic carbon isotope values and XRF Fe intensity data, following refs 35, 48.
454 The Palaeocene Carbon Isotope Maximum (PCIM); Early Late Palaeocene Event (ELPE);
455 Latest Danian Event (LDE) and the K/Pg boundary were identified in benthic carbon isotope
456 values and XRF Fe intensity data⁴⁸, and the positions of the PCIM and LDE were verified
457 against records from ODP Site 1262⁴⁹. The Lower C29n and Dan-C2 events are not clear in
458 the benthic carbon isotope data at ODP Site 1209⁴⁸, but were identified following ref 50, who
459 suggest that the peaks in magnetic susceptibility⁵¹ and XRF Fe intensity³⁵ identified as Pa2
460 and Pa1 by ref 35 correlate with the Lower C29n and Dan-C2 events, respectively. The
461 position of the Dan-C2 is consistent with estimates for the timing of this event^{34,52}.

462 **Relationships between variance and carbon isotope excursion magnitude.** For each
463 climate event we use the carbon isotope excursion (CIE) magnitude as a proxy for the level of
464 environmental perturbation, as illustrated by the scaling of temperature change with CIE size
465 for several of the Eocene hyperthermals⁵³. For the purposes of comparing environmental
466 perturbation and Σ_{CV} (Fig. 2), we plot magnitude of CIE using a combination of size of
467 excursion as recorded at ODP Site 1209 and the magnitude of excursion estimated from

468 published bulk carbon isotope data at globally distributed sites (Extended Data Table 2). We
469 used the maximum recorded excursion, except where this was inconsistent with other
470 available data. As well as values from bulk carbon isotope data (consistent with ref 21), we
471 took into account available benthic CIE values, which are arguably preferable for resolving
472 global signals⁵⁴. The value of carbon isotopes used for plotting non-event Σ_{CV} data points in
473 Figure 2 uses the deviation of the carbon isotope value from the detrended running average
474 (using an 11-point running average through non-event-only values), for a data-point every
475 ~150 kyr between climatic events. We regressed first differences in Σ_{CV} and first differences
476 in CIE magnitude (Fig. 2b) to statistically explore the relationship between community
477 stability and climate change across this 13-million-year interval, using a generalised least
478 squares framework (gls function in the nlme library in R) that applies best-fit models that
479 incorporate heteroscedastic (non-constant variance with the mean) and temporally auto-
480 correlated (time-series) errors.

481 **Milestones (Figure 3).** *Biological pump reboot (0.30 Myr) and recovery (1.77 Myr)*: Carbon
482 isotope records of benthic and planktonic foraminifera from Walvis Ridge (southern
483 Atlantic), adjusted to account for vital effects and ecology, show a crash in surface- to deep-
484 water carbon-isotope gradients at the mass extinction level and indicate that transfer of
485 organic matter to the deep-sea via the biological pump was severely perturbed⁹. These
486 records show that vertical gradients were close to zero for the initial 0.3 Myr after the
487 extinction, then slowly increased to attain pre-extinction levels at around 1.77 Myr. This is
488 interpreted as evidence that the duration of weakened biological pumping was no longer than
489 1.77 Myrs⁹, providing an estimate for full biological pump recovery. *Photosymbiosis and*
490 *depth partitioning in planktonic foraminifera (2.5 Myr)*: Based on reconstructions of the
491 palaeoecology of planktonic foraminifera using the oxygen and carbon stable isotopes of their
492 shells, the appearance of photosymbiosis and expansion of depth partitioning both occur
493 around 2.5 Myr after the mass extinction^{9,55}. *Appearance of oligotrophic coccolithophores*
494 *(3.5 Myr)*: The first appearance of early fasciculiths and sphenoliths represent the earliest
495 representatives of the Discoasterales group, which is largely characterized by oligotrophic
496 taxa (e.g., ref 28). The earliest representatives, *Fasciculithus magnus* and *F. magnicordis*,
497 appear at ~63 Myr ago (herein; ref 56) with other fasciculiths and sphenoliths following soon
498 after (62.13 and 61.98 Myr ago, according to ref 43).

499 **Selected taxonomic notes.** *Praeprinsius*: used here to include very small (<3 μ m) circular to
500 subcircular specimens of *Praeprinsius tenuiculum*. *Praeprinsius* is considered a synonym of
501 *Prinsius* by some, but we consider these groups to be morphologically distinct. *Fasciculithus*:
502 We use ‘early fasciculiths’ to include specimens that some may now identify as
503 *Gomphiolithus*, *Diantholitha*, and *Lithoptychius* (e.g., refs 56,58,59), while our main
504 ‘*Fasciculithus*’ group includes taxa that have been consistently classified within this genus,
505 e.g., *F. involutus* and *F. tympaniformis*. *Sphenoliths*: The earliest specimens of the genus
506 *Sphenolithus* (e.g., refs 56,60) are highly variable and we distinguish between the earliest
507 incoming specimens (termed ‘early sphenoliths’) and the main generic group ‘*Sphenolithus*’,
508 which includes *S. primus/moriformis* and *S. anarrhopus*.

509

510 **References for Methods and Extended Data**

- 511 33. Westerhold, T. & Röhl, U. Data report: Revised composite depth records for Shatsky
512 Rise Sites 1209, 1210, and 1211. in *Proceedings of the Ocean Drilling Program,*
513 *Scientific Results 198* (eds. Bralower, T. J., Premoli-Silva, I. & Malone, M. J.) 1–26
514 (2006).
- 515 34. Dinarès-Turell, J., Westerhold, T., Pujalte, V., Röhl, U. & Kroon, D. Astronomical
516 calibration of the Danian stage (Early Paleocene) revisited: Settling chronologies of
517 sedimentary records across the Atlantic and Pacific Oceans. *Earth Planet. Sci. Lett.*
518 **405**, 119–131 (2014).
- 519 35. Westerhold, T. *et al.* Astronomical calibration of the Paleocene time. *Palaeogeogr.*
520 *Palaeoclimatol. Palaeoecol.* **257**, 377–403 (2008).
- 521 36. Bown, P. R. & Young, J. R. Techniques. in *Calcareous Nannofossil Biostratigraphy*
522 (ed. Bown, P. R.) 16–28 (Chapman & Hall, 1998).
- 523 37. Perch-Nielsen, K. Cenozoic calcareous nannofossils. in *Plankton Stratigraphy* (eds.
524 Bolli, H. M., Saunders, J. B. & Perch-Nielsen, K.) 427–555 (Cambridge University
525 Press, 1985).
- 526 38. Bown, P. R. Paleocene calcareous nannofossils from Tanzania (TDP sites 19, 27 and
527 38). *J. Nannoplankt. Res.* **36**, 1–32 (2016).
- 528 39. Young, J. R., Bown, P. R. & Lees, J. A. Nannotax3 website. (2019). Available at:
529 <http://www.mikrotax.org/Nannotax3/>.
- 530 40. Bown, P.R., *et al.*, A Paleogene calcareous microfossil Konservat-Lagerstätte from the
531 Kilwa Group of coastal Tanzania. *Geol. Soc. Am. Bull.* **120**, 3–12 (2008)
- 532 41. Paillard, D., Labeyrie, L. & Yiou, P. Macintosh Program performs time-series
533 analysis. *Eos, Trans. Am. Geophys. Union* **77**, 379–379 (1996).
- 534 42. Cleland, E. E. Biodiversity and Ecosystem Stability. *Nature Education Knowledge*
535 **3**(10), 14 (2011).
- 536 43. *The Geologic Time Scale 2012*. (Elsevier, 2012).
- 537 44. Mai, H., Perch-Nielsen, K., Willems, H. & Romein, A. J. T. Fossil Cocospheres from
538 the K/T Boundary Section from Geulhemmerberg, the Netherlands. *Micropaleontology*
539 **43**, 281–302 (1997).
- 540 45. Mai, H., Hildebrand-Habel, T., Perch-Nielsen, K. V. S. & Willems, H. Paleocene
541 coccospheres from DSDP Leg 39, Site 356, Sao Paulo Plateau, S Atlantic Ocean. *J.*
542 *Nannoplankt. Res.* **20**, 21–29 (1998).
- 543 46. Gibbs, S. J., Sheward, R. M., Bown, P. R., Poulton, A. J. & Alvarez, S. Warm
544 plankton soup and red herrings: calcareous nannoplankton cellular communities and
545 the Palaeocene–Eocene Thermal Maximum. *Philos. Trans. R. Soc. A* 20170075 (2018).
546 doi:10.1098/rsta.2017.0075
- 547 47. Schmidt, A. *et al.* Selective environmental stress from sulphur emitted by continental
548 flood basalt eruptions. *Nat. Geosci.* **9**, 77–82 (2016).
- 549 48. Westerhold, T., Röhl, U., Donner, B., McCarren, H. K. & Zachos, J. C. A complete
550 high-resolution Paleocene benthic stable isotope record for the central Pacific (ODP

- 551 Site 1209). *Global Biogeochem. Cycles* **25**, 1–13 (2011).
- 552 49. Littler, K., Röhl, U., Westerhold, T. & Zachos, J. C. A high-resolution benthic stable-
553 isotope record for the South Atlantic: Implications for orbital-scale changes in Late
554 Paleocene-Early Eocene climate and carbon cycling. *Earth Planet. Sci. Lett.* **401**, 18–
555 30 (2014).
- 556 50. Coccioni, R. *et al.* The Dan-C2 hyperthermal event at Gubbio (Italy): Global
557 implications, environmental effects, and cause(s). *Earth Planet. Sci. Lett.* **297**, 298–
558 305 (2010).
- 559 51. Shipboard Scientific Party. Chapter 5: Site 1209. in *Proceedings of the Ocean Drilling*
560 *Program, Initial Reports 198* (eds. Bralower, T. J., Premoli-Silva, I. & Malone, M. J.)
561 1–102 (2002). doi:10.2973/odp.proc.ir.198.105.2002
- 562 52. Westerhold, T., Röhl, U., Frederichs, T., Bohaty, S. M. & Zachos, J. C. Astronomical
563 calibration of the geological timescale: Closing the middle Eocene gap. *Clim. Past* **11**,
564 1181–1195 (2015).
- 565 53. Stap, L. *et al.* High-resolution deep-sea carbon and oxygen isotope records of Eocene
566 Thermal Maximum 2 and H2. *Geology* **38**, 607–610 (2010).
- 567 54. Zeebe, R. E., Westerhold, T., Littler, K. & Zachos, J. C. Orbital forcing of the
568 Paleocene and Eocene carbon cycle. *Paleoceanography* **32**, 440–465 (2017).
- 569 55. Birch, H., Coxall, H. K. & Pearson, P. N. Evolutionary ecology of Early Paleocene
570 planktonic foraminifera: size, depth habitat and symbiosis. *Paleobiology* **38**, 374–390
571 (2012).
- 572 56. Monechi, S., Reale, V., Bernaola, G. & Balestra, B. The Danian/Selandian boundary at
573 Site 1262 (South Atlantic) and in the Tethyan region: Biomagnetostratigraphy,
574 evolutionary trends in fasciculiths and environmental effects of the Latest Danian
575 Event. *Mar. Micropaleontol.* **98**, 28–40 (2013).
- 576 57. Bralower, T. J. Paleocene-Early Oligocene calcareous nannofossil biostratigraphy,
577 ODP Leg 198 Sites 1209, 1210, and 1211 (Shatsky Rise, Pacific Ocean). in
578 *Proceedings of the Ocean Drilling Program, Scientific Results 198* (eds. Bralower, T.
579 J., Premoli Silva, I. & Malone, M. J.) 1–15 (2005).
- 580 58. Aubry, M.-P., Bord, D. & Rodriguez, O. New taxa of the Order Discoasterales Hay
581 1977. *Micropaleontology* **57**, 269–288 (2011).
- 582 59. Monechi, S., Reale, V., Bernaola, G. & Balestra, B. Taxonomic review of early
583 Paleocene fasciculiths. **58**, *Micropaleontology* 351–365 (2012).
- 584 60. Agnini, C. *et al.* High-resolution nannofossil biochronology of middle Paleocene to
585 early Eocene at ODP Site 1262: Implications for calcareous nannoplankton evolution.
586 *Mar. Micropaleontol.* **64**, 215–248 (2007).
- 587 61. van Heck, S. E. & Prins, B. A refined nannoplankton zonation for the Danian of the
588 Central North Sea. *Abhandlungen der Geol. Bundesanstalt* **39**, 285–303 (1987).
- 589 62. Sáez, A.G., Probert, I., Young, J.R., Edvardsen, B., Wenche, E. & Medlin, L.K. A
590 review of the phylogeny of the Haptophyta. in *Coccolithophores - from molecular*
591 *processes to global impact* (eds Thierstein, H.R. & Young, J.R.) 251-270 (Springer
592 2004).

- 593 63. Young, J.R., Geisen, M. & Probert, I. A review of selected aspects of coccolithophore
594 biology with implications for palaeobiodiversity estimation. *Micropaleontology*, **51**,
595 267-288 (2005).
- 596 64. Young, J.R., Liu, H., Probert, I., Aris-Brosou, H. & de Vargas, C. Morphospecies
597 versus phylopecies concepts for evaluating phytoplankton diversity: the case of the
598 Coccolithophores. *Cryptogamie, Algologie* **35**, 353-377 (2014).
- 599 65. Cramer, B. S., Wright, J. D., Kent, D. V. & Aubry, M. P. Orbital climate forcing of
600 $\delta^{13}\text{C}$ excursions in the late Paleocene-early Eocene (chrons C24n-C25n).
601 *Paleoceanography* **18**, 1–25 (2003).
- 602 66. Nicolo, M. J., Dickens, G. R., Hollis, C. J. & Zachos, J. C. Multiple early Eocene
603 hyperthermals: Their sedimentary expression on the New Zealand continental margin
604 and in the deep sea. *Geology* **35**, 699–702 (2007).
- 605 67. Lourens, L. J. *et al.* Astronomical pacing of late Palaeocene to early Eocene global
606 warming events. *Nature* **435**, 1083–1087 (2005).
- 607 68. Zachos, J. C. *et al.* A transient rise in tropical sea surface temperature during the
608 Paleocene-Eocene thermal maximum. *Science* **302**, 1551–4 (2003).
- 609 69. Zachos, J. C. *et al.* Rapid acidification of the ocean during the Paleocene-Eocene
610 Thermal Maximum. *Science* **308**, 1611–1615 (2005).
- 611 70. Bernaola, G. *et al.* Evidence of an abrupt environmental disruption during the mid-
612 Paleocene biotic event (Zumaia section, western Pyrenees). *Bull. Geol. Soc. Am.* **119**,
613 785–795 (2007).
- 614 71. Quillévéré, F., Aubry, M.-P., Norris, R. D. & Berggren, W. A. Paleocene
615 oceanography of the eastern subtropical Indian Ocean: An integrated
616 magnetobiostratigraphic and stable isotope study of ODP Hole 761B (Wombat
617 Plateau). *Palaeogeogr. Palaeoclimatol. Palaeoecol.* **184**, 371–405 (2002).
- 618 72. Arenillas, I., Molina, E., Ortiz, S. & Schmitz, B. Foraminiferal and $\delta^{13}\text{C}$ isotopic
619 event-stratigraphy across the Danian-Selandian transition at Zumaya (northern Spain):
620 Chronostratigraphic implications. *Terra Nov.* **20**, 38–44 (2008).
- 621 73. Bornemann, A. *et al.* Latest Danian carbon isotope anomaly and associated
622 environmental change in the southern Tethys (Nile Basin, Egypt). *J. Geol. Soc.*
623 *London.* **166**, 1135–1142 (2009).
- 624 74. Jehle, S., Bornemann, A., Deprez, A. & Speijer, R. Planktic foraminiferal response to
625 the Latest Danian Event in the Pacific Ocean (ODP Site 1210). **17**, 9115 (2015).
- 626 75. Schmitz, B. *et al.* High-resolution iridium, $\delta^{13}\text{C}$, $\delta^{18}\text{O}$, foraminifera and nannofossil
627 profiles across the latest Paleocene benthic extinction event at Zumaya, Spain.
628 *Palaeogeogr. Palaeoclimatol. Palaeoecol.* **133**, 49–68 (1997).
- 629 76. Schmitz, B., Molina, E. & von Salis, K. The Zumaya section in Spain: A possible
630 global stratotype section for the Selandian and Thanetian stages. *Newsletters Stratigr.*
631 **36**, 35–42 (1998).
- 632 77. Kroon, D., Zachos, J. C. & Leg 208 Scientific Party. Cenozoic climate cycles and
633 excursions. in *Proceedings of the Ocean Drilling Program, Scientific Results 208* (eds.
634 Kroon, D., Zachos, J. C. & Richter, C.) 1–55 (2007).

635 doi:10.2973/odp.proc.sr.208.201.2007

636 78. Quillévéré, F., Norris, R. D., Kroon, D. & Wilson, P. A. Transient ocean warming and
637 shifts in carbon reservoirs during the early Danian. *Earth Planet. Sci. Lett.* **265**, 600–
638 615 (2008).

639 **Acknowledgments** This research used samples provided by the International Ocean
640 Discovery Program. We would like to thank the Royal Society for funding S.J.G. through a
641 URF. R.M.S. was funded jointly through a Vice Chancellor's studentship from the University
642 of Southampton and a Natural Environment Research Council (NERC) studentship (award
643 reference 1272561), and H.K. was part supported by a UCL Dean's prize. We would also like
644 to thank the European Union for post-doctoral research funding for S.A.A. (grant ERC-2013-
645 CoG-617303). A.R. was partly supported by an award from the Heising-Simons Foundation
646 as well as via grant ERC-2013-CoG-617303. We would like to thank Tom Ezard for
647 contributions to the interpretation of the datasets and Paul Wilson for his independent editing
648 of the manuscript.

649 **Author contributions** S.J.G., P.R.B. and A.R. conceived and designed the study. S.A.A.
650 developed the methodology and performed the majority of data collection. S.A.A. and S.J.G.
651 performed the data analyses. P.R.B., R.M.S., H.K. and A.R. contributed to data collection,
652 analysis and interpretation. S.J.G. and P.R.B. wrote the manuscript and A.R., S.A.A. and
653 R.M.S. participated in manuscript writing and editing.

654 **Author Information** Reprints and permissions information is available at
655 www.nature.com/reprints. The authors declare no competing interests. Correspondence and
656 requests for materials should be addressed to S.A.A. (sarah.alvarez@unigib.edu.gi) or S.J.G.
657 (sxg@noc.soton.ac.uk).

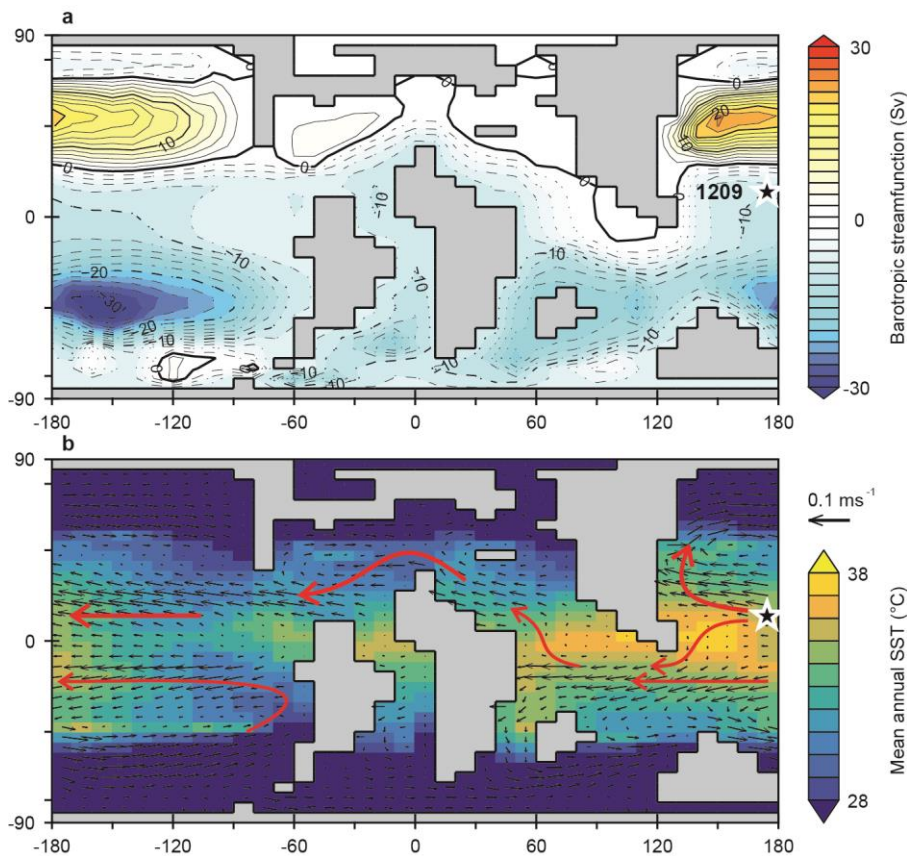
658 **Data availability** The datasets generated or analysed during this study are included in the
659 published article, linked directly to figures 1, 2 and 3.

660

661

662 **Extended data figures:**
663 **Extended Data Figure 1. Location of ODP Site 1209 (black star) with respect to model**
664 **simulated late Cretaceous major ocean current and circulation patterns. a,** Barotropic
665 streamfunction simulated in a late Cretaceous configuration of the *c*GENIE Earth system
666 model⁴⁷. **b,** Surface ocean current field (black arrows) for the same circulation state as **(a)**
667 overlain on annual average ocean surface temperature (colours). Scale for current vectors on
668 the right, along with a truncated temperature scale to highlight distribution of comparable
669 temperature regimes. Red arrows illustrate inferred flow paths relevant to the position of
670 ODP Site 1209 (marked by a star).

671

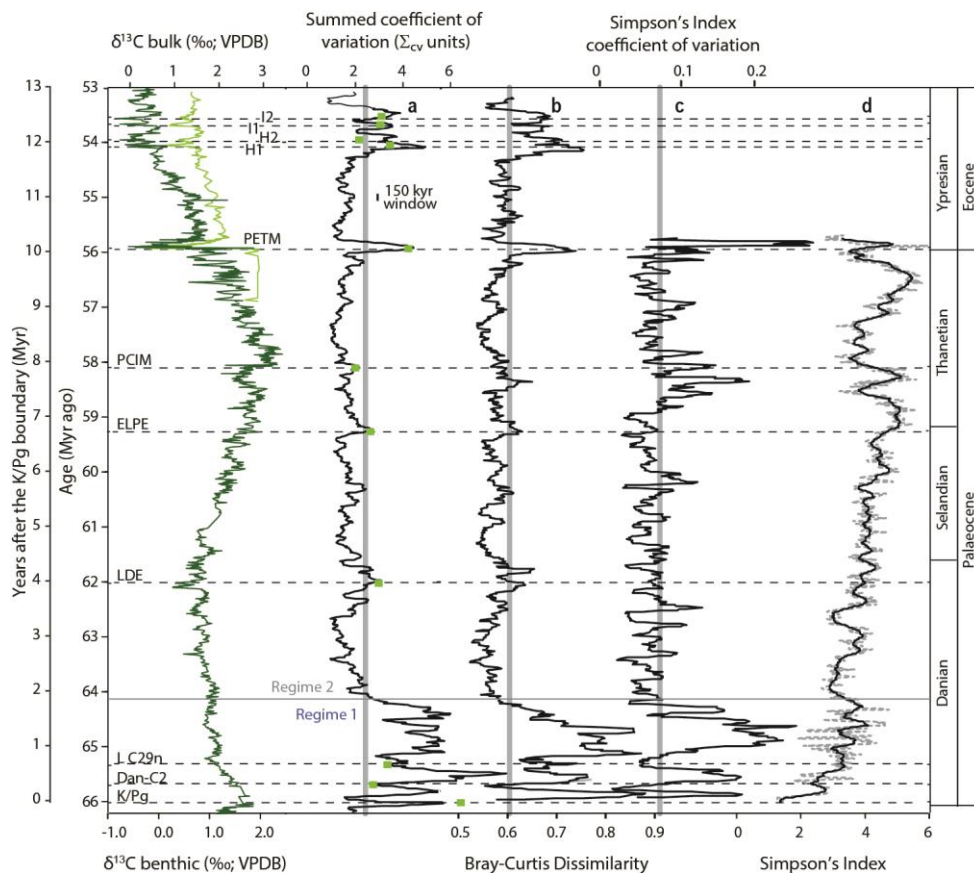


672

673

674 **Extended Data Figure 2. Comparison of community structure metrics.** Downcore plots
 675 of (a) Σ_{CV} , (b) Bray-Curtis dissimilarity (BC), (d) Simpson's index (SI, grey dashed lines,
 676 150 kyr moving average – black line) and the variance (150 kyr window) in the SI (c).
 677 Vertical grey lines on a and b show the level of background inferred from rank order plots of
 678 these data. All four metrics (Σ_{CV} , BC, SI and SI-variance) show volatility distinction between
 679 early Danian Regime 1 (n = 137 data points) and Regime 2 (the rest of the record, n = 861
 680 data points), e.g., the Wilcoxon Rank Sum value for the Simpson's record = 46646, $p < 0.001$
 681 on first differences, with 95% confidence limits of -0.013, -0.006. A W value of zero would
 682 support a null hypothesis. The test was two-sided. SI shows a diversity minimum in the
 683 earliest Danian and then a rapid increase and steady long-term trend towards more diverse,
 684 more even communities, but with high variability in the early Danian. This SI fluctuation, as
 685 recorded by the record's variance (c) shows similar patterns to BC and Σ_{CV} with high
 686 variance in the early Danian before dropping down. SI variance also shows high background
 687 fluctuations and a sustained rise in amplitude of fluctuations around the PCIM isotope shift,
 688 reflecting oligotroph diversification, which the SI shows strongly due to its higher sensitivity
 689 to rare taxa. In effect, metric sensitivity to taxic richness and rare taxa increases from panel a
 690 to c (from abundance variance to diversity variance). Note – SI can only be performed on full
 691 assemblage data and therefore the record only extends up to 55.5 Myr ago.

692

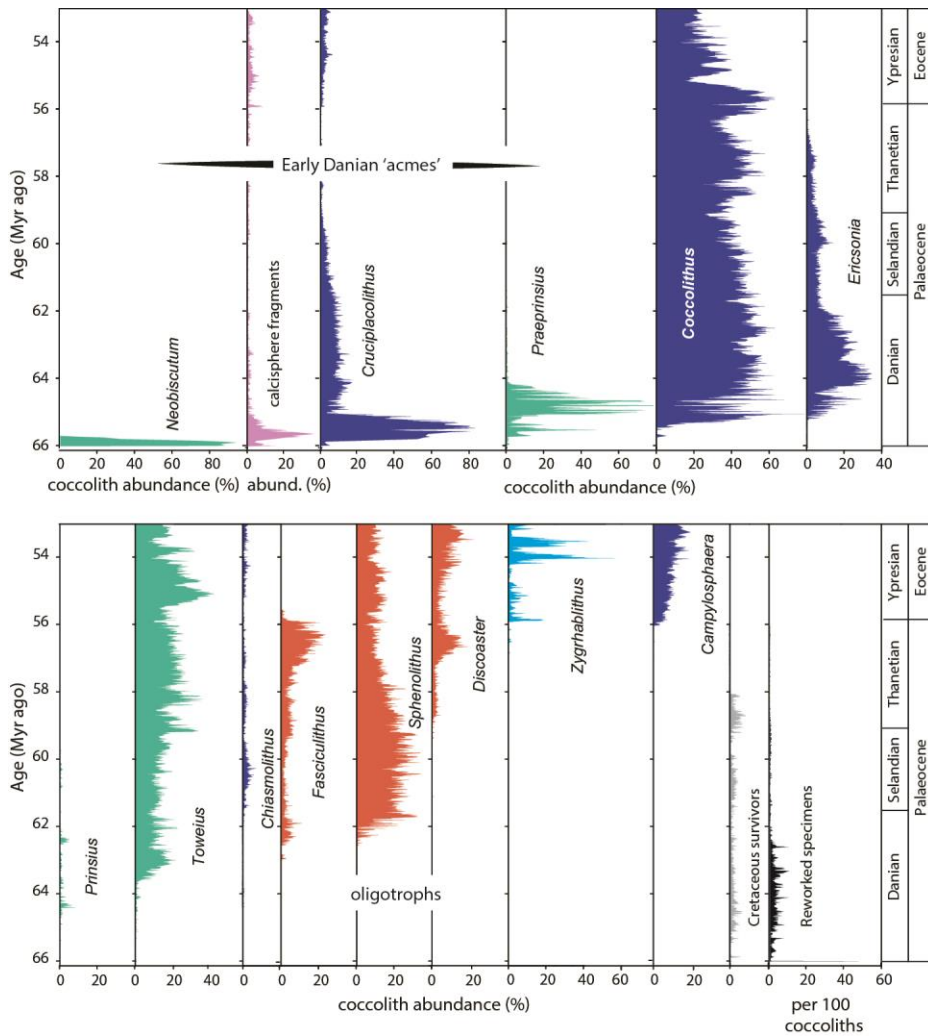


693

694

695 **Extended Data Figure 3. Relative abundance of key nannoplankton groups and**
 696 **abundance of reworked specimens per 100 nannofossils.** Relative abundance of coccoliths
 697 from all groups included in the Σ_{CV} metric are shown, coloured according to clade (as per
 698 Fig. 1b) and ordered by stratigraphic appearance. Cretaceous survivor taxa were counted as
 699 individual species but have been grouped together here, comprising mostly *Zeugrhabdotus*
 700 with lower abundances of *Cyclagelosphaera*, *Markalius* and *Neocrepidolithus*.

701

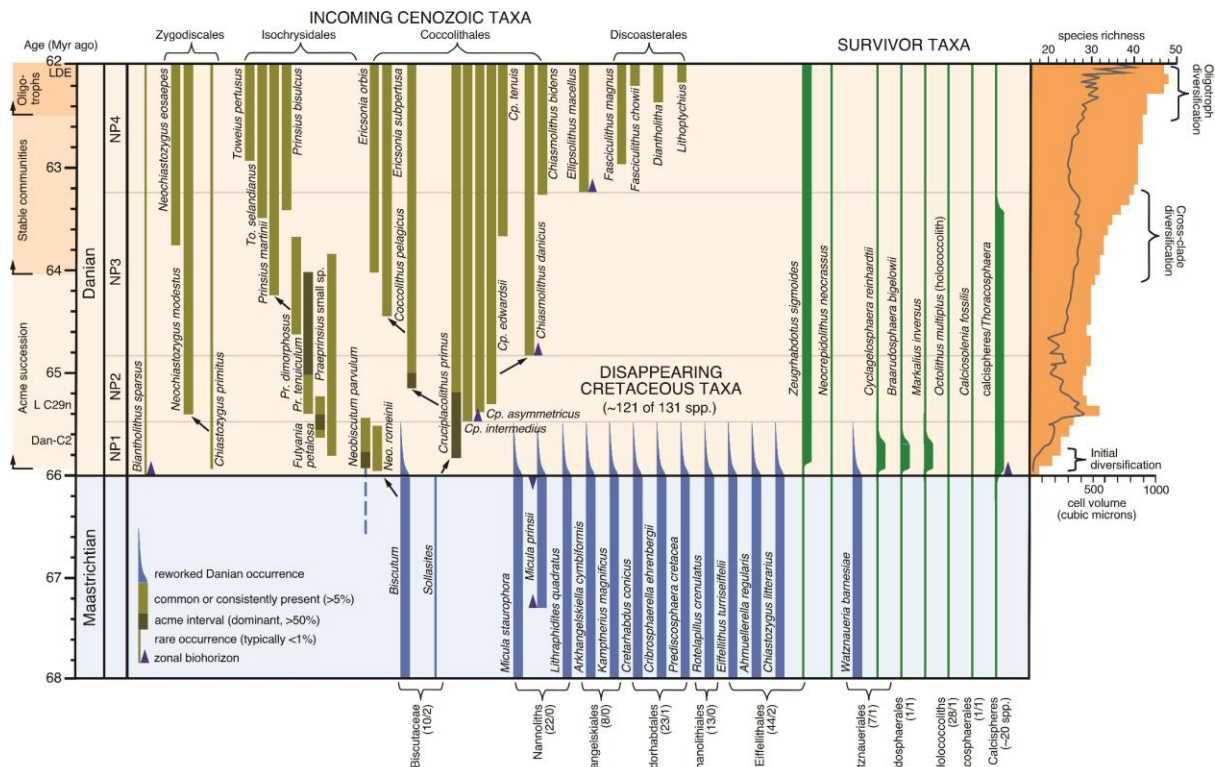


702

703

704 **Extended Data Figure 4. Calcareous nannoplankton across the K/Pg boundary.**
 705 Stratigraphic distribution of significant species grouped as incoming (brown), survivor (green)
 706 (green) or disappearing taxa (blue). A subset of Cretaceous taxa are shown, with latest
 707 Maastrichtian diversity for families shown alongside number of survivors. Gradualistic
 708 evolutionary transitions indicated by close spacing and arrows indicate genus-level
 709 transitions. The nannoplankton data are primarily from our work but are largely consistent
 710 with published sources (e.g., refs 10,15,16,37,61). Diversity and cell-volume records from
 711 Figure 3. *Cp.* = *Cruciplacolithus*, Dan-C2, L C29n = hyperthermals, LDE = late Danian event,
 712 *Neobisc.* = *Neobiscutum*, NP = nanofossil biozone, *Prae.* = *Praeprinsius*.

713

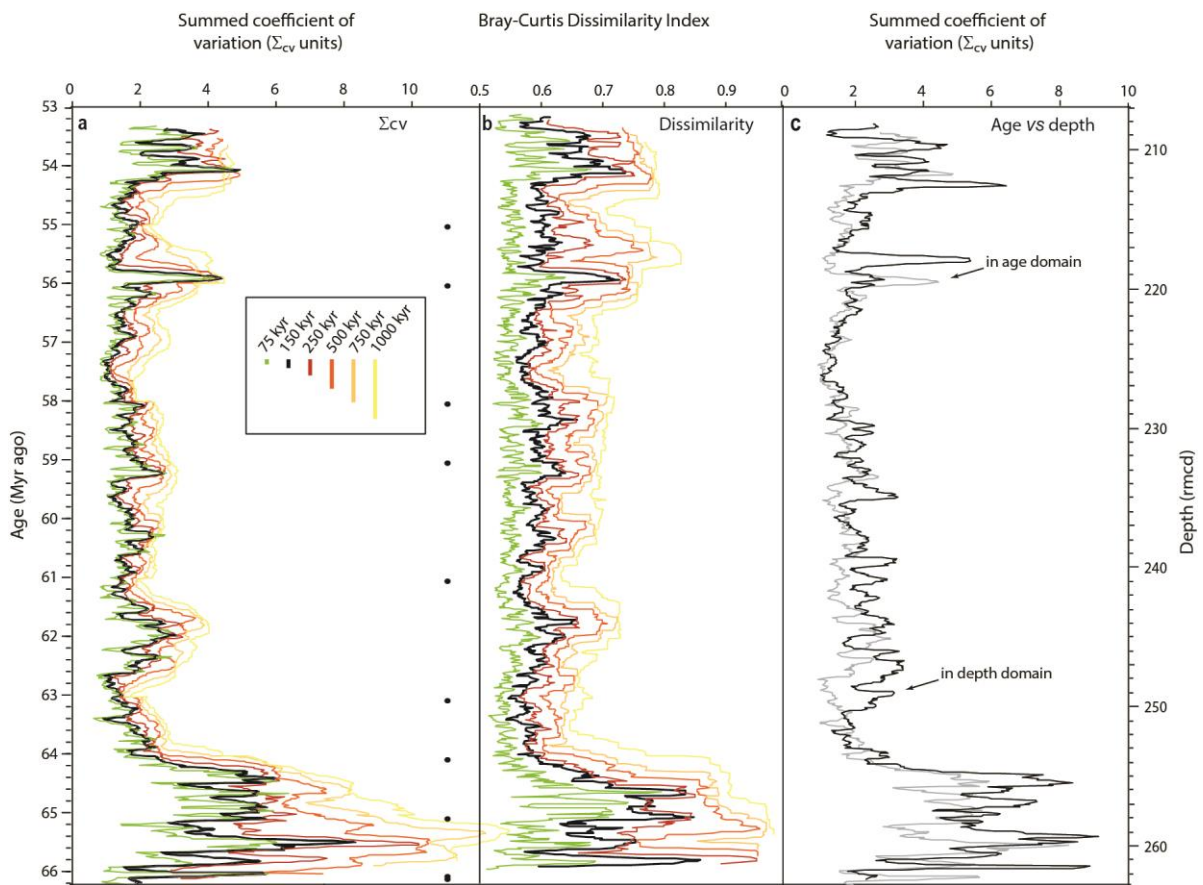


714

715

716 **Extended Data Figure 5. Impact of (a) window duration and (c) sampling in either the**
 717 **depth or age domain on the summed coefficient of variability (Σ_{CV}), and impact of**
 718 **window duration on Bray-Curtis dissimilarity (BC) (b). a, b, Σ_{CV} and BC calculated using**
 719 **different window durations (75-1000 kyr). c, side-by-side results of Σ_{CV} calculated using**
 720 **evenly spaced samples in either the depth domain or the age domain using a depth window**
 721 **duration of 60 cm, which is broadly equivalent to the 150 kyr time window. When Σ_{CV} is**
 722 **plotted in the depth domain the main patterns are retained, indicating that no significant**
 723 **artefacts arise from the applied age model. The boundaries between the million-year sections,**
 724 **where the taxa included in the Σ_{CV} change (black dots) are also marked on panel a and again**
 725 **there are no obvious artefacts across the million year windows with changes in the most**
 726 **abundant taxa.**

727

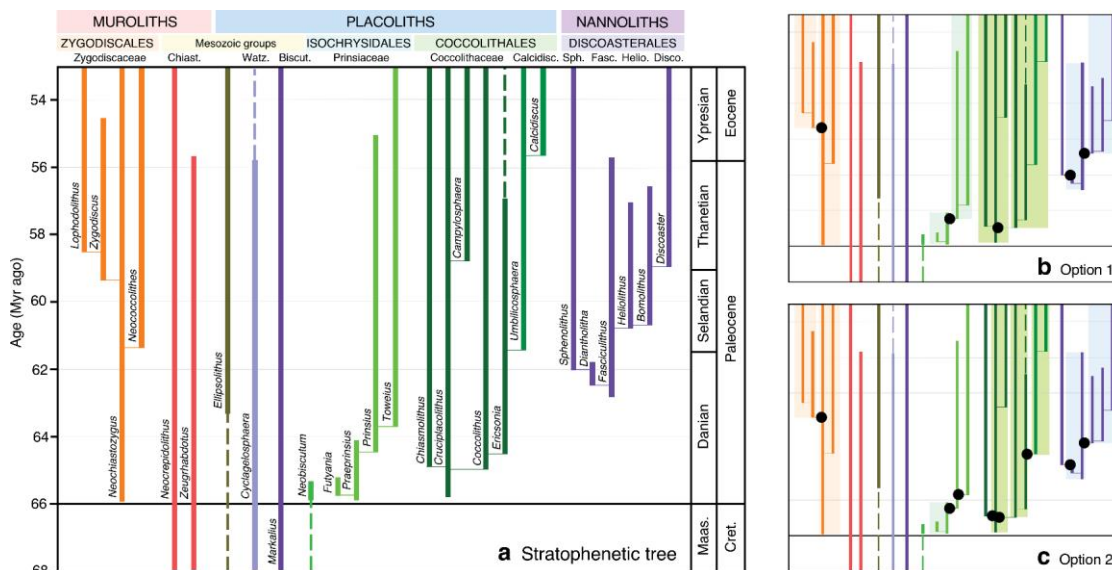


728

729

730 **Extended Data Figure 6. Phylogenetic models for the dominant Paleocene**
 731 **nannoplankton.** Models range from a standard genus-level stratophenetic tree (**a**) through
 732 two successively conservative scenarios (**b, c**) grouping closely-related taxa, i.e., recently
 733 diverged taxa based on morphological and stratigraphic range data. Nannoplankton taxonomy
 734 is primarily based on the morphology and crystallographic ultrastructure of exoskeletal
 735 coccoliths but the addition of genetic data for modern taxa has confirmed that this approach is
 736 robust^{62,63,64}. Evolutionary models are stratophenetic because we have high-quality
 737 stratigraphic information but lack the range of meaningful homologous morphological
 738 characters to allow a cladistic analysis. **a**, genus-level phylogeny based on an extensive
 739 species-level stratophenetic tree. **b** and **c** are different ancestry options used to test for
 740 artefacts and sensitivity in variance/dissimilarity that may result from equal weighting of
 741 closely-related versus more distantly-related taxa. **b**, ancestry model option 1 is highly
 742 conservative and merges major sub-family groups (shown by shaded boxes) about five nodes
 743 shown by black circles. **c**, ancestry model option 2 merges the most closely-related genera
 744 (shaded boxes) about eight nodes.

745

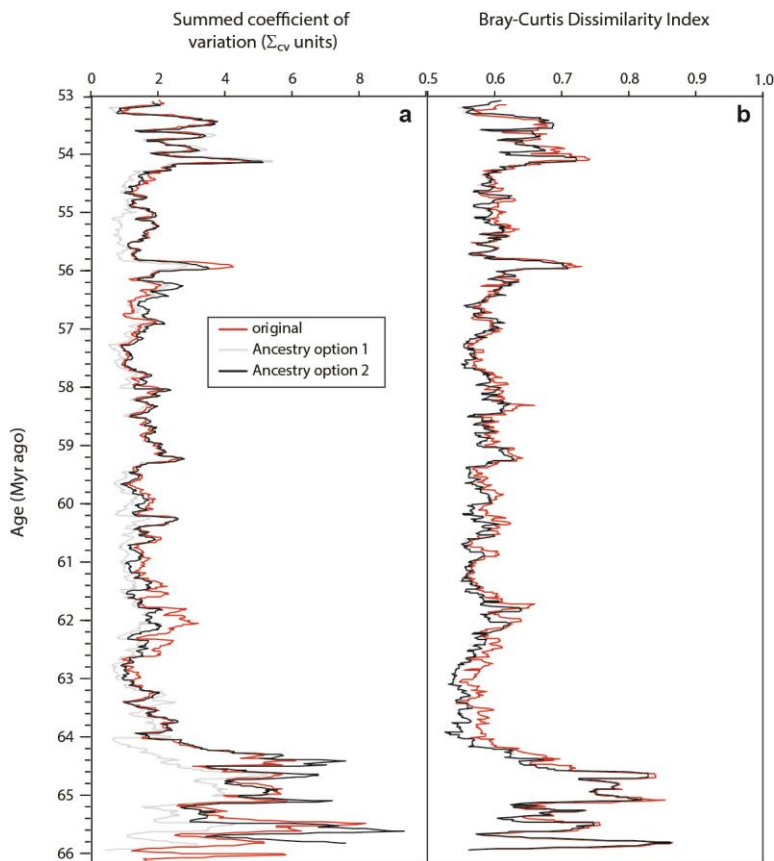


746

747

748 **Extended Data Figure 7. Impact of ‘ancestry’ on (a) summed coefficient of variability**
749 **(Σ_{cv}) and (b) Bray-Curtis dissimilarity (BC).** Analyses of the dataset applying two
750 additional models of shared ancestry using the reconstructed genus-level stratophenetic tree
751 in Extended Data Figure 6a. In red, the original analysis giving each genus equal. In grey,
752 analysis of the conservative ancestry model that merges genera into major sub-family groups
753 (ancestry model option 1, Extended Data Fig. 6b). In black, analysis of the moderately
754 conservative ancestry model option 2 (Extended Data Fig. 6c) which merges the most
755 closely-related genera. BC displays very little sensitivity to varying the taxonomic
756 hierarchies. Σ_{cv} displays some sensitivity, particularly at the Late Danian Event (around 62
757 Myrs ago) but the main patterns are retained between the original and option 2. Some
758 variance is lost in the less realistic option 1 analysis, where grouping of key genera that lie in
759 the same families dampens the variance, in particular, in the early Danian. However, the early
760 Danian variance values still remain anomalously high compared to the rest of the record.

761



762

763

764 **Extended Data Table 1. Summary of main biometric lith and cell parameters measured**
 765 **and reconstructed.** C_N is the number of coccoliths per cell, Θ is cell diameter, and C_L is lith
 766 length. Sites referred to include ODP Site 1209 and IODP Sites 1403 and 1407. ‘Pg
 767 coccospheres’ refers to new coccosphere measurements for the Palaeogene. SEM images of
 768 published coccospheres are all from refs 44,45.

769

Clade	Taxon	Lith number (C_N)	Cell size (Θ , μm)	Cell volume (μm^3)	Source
Cretaceous survivors	<i>Neocrepidolithus</i>	32.5	16.5	2352	Ref. 46
	<i>Zeugrhabdotus</i>	32.5	16.5	2352	Ref. 46
	<i>Markalius</i>	12	8.3	297	Pg coccospheres
	<i>Cyclagelosphaera</i>	12	7.9	259	C_N from published SEM images; Θ estimated from lith measurements at Sites 1209, 1403 and published coccosphere images. Geometry consistent with Pg coccospheres
Coccolithales	<i>Chiasmolithus</i>	9	11.0	698	Pg coccospheres
	<i>Coccolithus</i>	13	7.0-9.7	180-478	C_N from Pg coccospheres; Θ change through Danian estimated from lith measurements at Sites 1209 and 1403 using geometric relationship from Pg coccospheres
	<i>Cruciplacolithus</i> (small)	20	4.2-8.0	39-268	C_N and Θ from Pg coccospheres and published coccosphere images; Θ change through Danian estimated from lith measurements from Sites 1209 and 1403 using geometric relationship from Pg coccospheres.
	<i>Cruciplacolithus</i> (large)	13	6.6-11.5	151-796	As for <i>Cruciplacolithus</i> (small), but considered to be more like <i>Chiasmolithus</i>
	<i>Ericsonia</i>	13	7.6	226	As for <i>Coccolithus</i>
Isochrysidales	<i>Neobiscutum</i>	9	3.0	14	Direct measurements of Danian coccospheres and estimates of Θ based on lith measurements from Sites 1209, 1403 and 1406.
	<i>Praeprinsius</i>	18	3.8-5.2	29-74	Direct measurements of Danian coccospheres and estimates of Θ change through Danian based on lith measurements from Sites 1209, 1403 and 1406.
	<i>Futyania</i>	50	8.5	322	Pg coccospheres and published coccosphere images
	<i>Prinsius</i>	20	4.0-5.5	34-87	Direct measurements of Danian coccospheres and estimates of Θ change through Danian based on lith measurements from Sites 1209, 1403 and 1406.
	<i>Toweius</i>	7	4.7	31	C_N from Pg coccospheres; Θ estimated from lith measurements from Sites 1209 and 1403 using geometric relationship from Pg coccospheres.
Zygodiscales	<i>Neochiastozygus</i>	32.5	16.5	2352	Ref. 46
Discoasterales	<i>Fasciculithus</i> ,	42	21.7	5350	Ref. 46
	<i>Sphenolithus</i>				
Incertae	<i>Biantholithus</i>	13	13.7	1337	Pg coccospheres
Non-nannofossil	Calcisphere fragments	16	20.0	4189	Pg coccospheres

770

771

772 **Extended Data Table 2. Carbon isotope excursion events.** Columns provide event
 773 nomenclature, depth in core at Site 1209, age and estimated size of the CIE. Values in
 774 parentheses show the range of CIEs from the literature cited and the value in bold is the size
 775 of CIE used in Figure 2. Event nomenclature follows references given in the Methods, depths
 776 (rmcd – revised metres composite depth) use the revised depth splice of ref 33 and the ages
 777 use the age model from ref 32.

778

Event	Depth (rmcd, splice)	Age (Myrs ago)	Size of CIE (‰)	References
I2	210.02	53.55	0.48 [0.1 – 0.6]	21,65,66.
I1	210.60	53.67	0.65 [0.5 – 0.7]	21,65,66.
H2	211.83	53.95	0.49 [0.2 – 0.6]	21,51,65,66.
H1	212.48	54.05	1.5 [0.6 – 1.6]	21,51,65–67.
PETM	218.00	55.93	3.0 [2.4 – 3]	68,69.
PCIM	229.94	58.10	1.0	48,49.
ELPE	235.00	59.27	0.75	48,49,72.
LDE	247.69	62.03	1.0	48,71–76.
L C29n	258.83	65.34	0.7	50,77.
Dan C2	260.11	65.71	1.3	50,77,78.

779